



Since January 2020 Elsevier has created a COVID-19 resource centre with free information in English and Mandarin on the novel coronavirus COVID-19. The COVID-19 resource centre is hosted on Elsevier Connect, the company's public news and information website.

Elsevier hereby grants permission to make all its COVID-19-related research that is available on the COVID-19 resource centre - including this research content - immediately available in PubMed Central and other publicly funded repositories, such as the WHO COVID database with rights for unrestricted research re-use and analyses in any form or by any means with acknowledgement of the original source. These permissions are granted for free by Elsevier for as long as the COVID-19 resource centre remains active.



Analogue discovery of safer alternatives to HCQ and CQ drugs for SAR-CoV-2 by computational design

Meetali Sinha^{a,b}, Anshika Gupta^a, Shristee Gupta^a, Prakrity Singh^{a,b}, Shraddha Pandit^{a,b}, Shweta Singh Chauhan^{a,b}, Ramakrishnan Parthasarathi^{a,b,*}

^a Computational Toxicology Facility, CSIR- Indian Institute of Toxicology Research, Vishvighyan Bhavan, 31, Mahatma Gandhi Marg, Lucknow 226001, Uttar Pradesh, India

^b Academy of Scientific and Innovative Research (AcSIR), Ghaziabad 201002, Uttar Pradesh, India

ARTICLE INFO

Keywords:

SARS-CoV-2
Hydroxychloroquine
Chloroquine
Analogues
In silico
Drug design

ABSTRACT

COVID-19 outbreak poses a severe health emergency to the global community. Due to availability of limited data, the selection of an effective treatment is a challenge. Hydroxychloroquine (HCQ), a chloroquine (CQ) derivative administered for malaria and autoimmune diseases, has been shown to be effective against both Severe Acute Respiratory Syndrome (SARS-CoV-1) and SARS-CoV-2. Apart from the known adverse effects of these drugs, recently the use of CQ and HCQ as a potential treatment for COVID-19 is under flux globally. In this study, we focused on identifying a more potent analogue of HCQ and CQ against the spike protein of SAR-CoV-2 that can act as an effective antiviral agent for COVID-19 treatment. Systematic pharmacokinetics, drug-likeness, basicity predictions, virtual screening and molecular dynamics analysis (200 ns) were carried out to predict the inhibition potential of the analogous compounds on the spike protein. This work identifies the six potential analogues, out of which two compounds, namely 1-[1-(6-Chloroquinolin-4-yl) piperidin-4-yl]piperidin-3-ol and (1R,2R)-2-N-(7-Chloroquinolin-4-yl)cyclohexane-1,2-diamine interact with the active site of the spike protein similar to HCQ and CQ respectively with augmented safety profile.

1. Introduction

Coronavirus Disease-2019 (COVID-19), triggered by severe acute respiratory syndrome coronavirus 2 (SARS-CoV-2), rapidly became a global pandemic and was reported from more than 200 countries. The outbreak of COVID-19 emerges as a serious risk to public health [1]. As of January 12, 2021, there have been more than 89 million cases of COVID-19 globally, including 1,940,352 deaths reported (<https://covid19.who.int/>). Such a massive number of infections and fatalities, calls for an imperative development of an effective treatment and affordable therapeutics to recover from the pandemic. FDA approved the use of chloroquine (CQ) and hydroxychloroquine (HCQ) as antimalarial and also for autoimmune diseases, for the treatment of COVID-19 patients as Emergency Use Authorization (EUA) with cautions issued afterwards [2–4].

CQ and HCQ are analogous chemical compounds whose mechanisms as a weak base and immunomodulatory properties are the same. Several studies have suggested the role of CQ in inhibiting viral entry,

replication, and post-translational modification [5–11]. Two different mechanisms have been reported on the role of CQ in inhibiting viral entry. These drugs act on the biosynthesis of sialic acid by inhibiting quinone reductase 2 [12,13] and simultaneously interacting with angiotensin-converting enzyme 2 receptors (ACE2), and impacting glycosylation [14,15]. CQ also interrupts the replication of the virus by increasing endosomal pH, thereby inhibiting virus-endosome fusion [16]. CQ also interferes with proteolytic processes and hampers post-translational modifications of viral proteins [17]. Similarly, HCQ also interferes with glycosylation, endosomal fusion, and lysosomal activity by modulating pH [18]. HCQ also impacts the signaling of Toll-like receptors (TLRs) by increasing endosomal pH. Immunomodulatory effects of HCQ suppresses major histocompatibility complex (MHC) class II expression by inhibiting T cell activation, expression of CD145, and release of cytokines [19].

An excessive dose of CQ reportedly causes acute poisoning and death [20]. HCQ, an analogue of CQ, developed with a hydroxyl group into CQ was much less toxic than its parent compound [21]. Recent reports have

* Corresponding author. Computational Toxicology Facility, CSIR- Indian Institute of Toxicology Research, Vishvighyan Bhavan, 31, Mahatma Gandhi Marg, Lucknow 226001, Uttar Pradesh, India.

E-mail address: partha.ram@iitr.res.in (R. Parthasarathi).

<https://doi.org/10.1016/j.combiomed.2021.104222>

Received 16 August 2020; Received in revised form 13 January 2021; Accepted 13 January 2021

Available online 20 January 2021

0010-4825/© 2021 Elsevier Ltd. All rights reserved.

indicated that the administration of HCQ also resulted in potential adverse effects on dermatomyositis patients and caused retinal toxicity [22,23]. Due to the adverse effects of HCQ and CQ and taking into consideration the treatment, there is a necessity to develop a potentially safer analogue of these drugs with no or minimal side effects. We developed an *in silico* framework for the discovery of analogue compounds and to identify potentially safer alternatives of CQ and HCQ using virtual screening and molecular dynamics simulations. Virtual screening was carried out in this study by the generation of potent analogues and molecular docking of the selected ligand library against the crystal structure of SARS-CoV-2 spike protein that exhibits inhibitory binding as antiviral, drug-likeness and safety profiling to treat COVID-19 infection and progression.

2. Computational details

2.1. Generation of analogous library

CQ and HCQ have been reported to have a possible inhibitory effect on the entry of SAR-CoV-2 in the host cell. Structural analogues of these two quinolone molecules were collected from the ZINC drug-like database [24] of the webserver SwissSimilarity [25]. To derive a potential alternative of these compounds, we used the SwissSimilarity web-based tool (<http://www.swissSimilarity.ch/>), which offers the possibility to perform Ligand Based Virtual Screening. The small molecules libraries cover drugs, bioactive compounds, commercially available molecules and virtual libraries. The molecules most similar to the reference compound are searched, along with the similarity score. The similarity-based virtual screening infers that all the chemicals extracted from the database are similar in the structure to the compound under query and have comparable biological properties vis-à-vis activities [26]. Tanimoto coefficient (T) is the most standard similarity measure for matching chemical structures. Screened structures are generally considered similar if their Tanimoto coefficient is greater than eighty-five percent. Their three-dimensional structure was downloaded in the structure data format (SDF) from the PubChem database [27], which was then converted into Protein Data Bank (PDB) file format using the Open Babel (http://openbabel.org/wiki/Main_Page).

2.2. Drug-likeness prediction/assessment

The SwissADME, an open-source tool, uses the Simplified molecular-input line-entry system (SMILE) to calculate various pharmacological properties. The drug-likeness screening of the Swiss ADME includes six rule-based methods such as Lipinski rule-of-five, Ghose filter, Veber Rule, Egan rule and Muegge filter which were applied for the selection of potent analogue for CQ and HCQ [28].

2.3. ADMET prediction

ADMET (Absorption, Distribution, Metabolism, Excretion & Toxicity) is vital in assessing the pharmacodynamics activities of the analogue. Several computational tools are available to predict and analyze ADMET profiles of the drug-like molecules. In this study, the following pharmacokinetics properties [29] namely, Blood-Brain Barrier (BBB), Human Intestinal Absorption (HIA), P-glycoprotein inhibitor, CYP450 inhibitory promiscuity (CYP) inhibitor, and carcinogenicity of the ligands were predicted using admetSAR server [30] (<http://lmmd.ecust.edu.cn/admetSAR2/>).

2.4. Protein target selection

Among all the 29 viral protein targets found in SAR-CoV-2, the spike protein was selected as it is found to have a potential role in the entry of the virus inside the host [31]. The crystal structure of the novel coronavirus spike receptor-binding domain complexed with its receptor

Angiotensin-Converting Enzyme 2 (ACE2) (PDB: 6LZG, 2.5 Å) [32] was obtained from the Research Collaboratory for Structural Bioinformatics Protein Data Bank (RCSB-PDB) [33]. SARS-CoV-2 spike protein is a heterodimer, consisting of chains A and B. For the molecular docking experiment, the hACE2 protein (chain A) was deleted and chain B from the PDB file of the complex was used. Also, all non-standard residues including water moieties were removed using Discovery Studio [34].

2.5. Molecular docking

Molecular docking was performed using AutoDockTools-1.5.6 [35]. Polar hydrogens and Kollman charges were added to the protein and a pdbqt format file was saved. The pdbqt files of each ligand were generated after adding all hydrogen and Kollman charges to each structure. The grid box was set for protein as 90 x 90 x 90 with 0.653 Å spacing to perform a blind (full coverage of the spike protein and complexes) docking simulations. Ten Lamarckian Genetic Algorithm runs were carried out for each ligand. For all the other parameters of docking, default settings were used. All the computational runs were carried out on Cygwin [36] for the generation of both grid parameter file (.gpf file) and a docking parameter file (.dpf file) for each specific ligand. The docked conformations of each ligand were selected based on binding affinity and the top-ranking conformations. The best-selected poses were then visualized using BIOVIA Discovery Studio [34].

2.6. Molecular dynamics (MD) simulation

MD simulations of the potent lead compounds, CQ1 and HCQ1 along with their parent drugs CQ and HCQ were carried out using GROMACS 5.1.4 [37]. The spike glycoprotein topology file was prepared by using the GROMOS96 43a1 force field. The ligand (CQ, CQ1, HCQ, HCQ1) topology files were built using the PRODRG server [38]. These complexes were solvated using SPC water models in a dodecahedron periodic box with boundaries extending nearly 10 Å in all directions. The counter ions were added to neutralize the total charge of the system. The steepest descent algorithm followed by conjugate gradient protocol for 50,000 steps with a cut-off value of 1000 kJ·mol⁻¹ was applied for energy minimization [39]. Equilibration of the four complexes was performed in two steps: NVT and then NPT for a period of 100ps each. Temperature coupling with a V-rescale was performed at a temperature of 300 K and a time constant of 0.1 ps, and pressure coupling was done with a Berendsen bath with a time constant 2.0 ps [40]. The Linear Constraint Solver (LINCS) algorithm was used to constrain the bond lengths of heavy atoms [41]. Finally, a 200 ns production run was performed. The coordinate trajectories were saved every 2 ps for the entire time-period [42]. The molecular dynamics analysis was conducted using gmx rms, gmx rmsf, gmx gyrate, gmx sasa, gmx covar, and gmx anaef module of the Gromacs package.

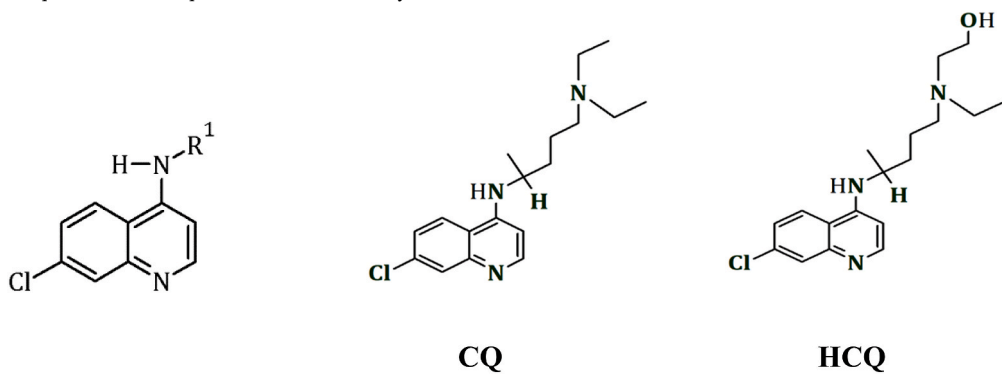
The principal components analysis of the spike-protein was performed by diagonalizing and solving the eigenvalue (represents the magnitude of motion along with the direction) & eigenvectors (represents of the direction of the motion) for the covariance matrix [43] to obtain functional motions for bio-molecules. Free energy landscape (FEL) represents possible conformations taken by a protein in MD simulation and the Gibbs free energy was calculated using probability distribution from the essential plane composed of the first two eigenvectors. The free energy is plotted along the two order parameters such as RMSD and Rgyr [44] to obtain FEL of the complexes simulated in this investigation. gmx sham tool was used for the construction of FEL.

2.7. Basicity prediction

Basicity and acidity of the drugs determine their functional role in targeting endosomal acidification in the biological system, particularly in modulating pH of CQ and HCQ for inhibiting viral replication [45]. The geometry optimizations of CQ and HCQ and their respective

Table 1

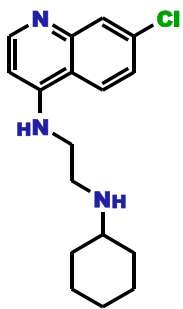
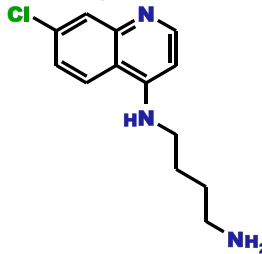
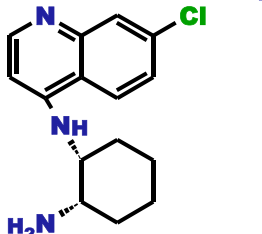
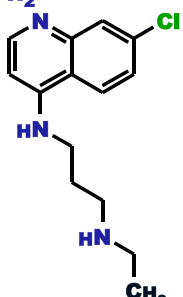
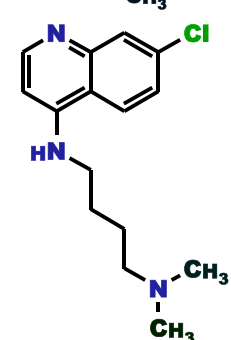
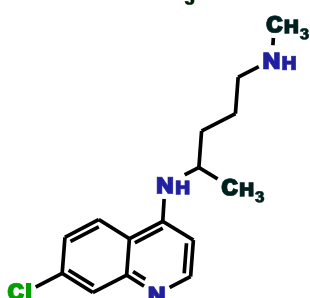
Analogues of Hydrochloroquine and Chloroquine with their similarity score.



Compounds	IUPAC Name & ZINC Id	PubChem CID	Tanimoto Coefficient	Chemical Structures
HCQ1	1-[1-(6-Chloroquinolin-4-yl)piperidin-4-yl]piperidin-3-ol ZINC95367069	72876338	0.886	
HCQ2	1-(7-chloroquinolin-4-yl)piperidin-4-ol ZINC40412048	60631468	0.883	
HCQ3	2-[4-(7-Chloroquinolin-4-yl) morpholin-2-yl] ethanamine ZINC32509033	45177282	0.871	
HCQ4	[1-(7-Chloroquinolin-4-yl)piperidin-3-yl] methanol ZINC40412383	60413266	0.869	
CQ1	1R,2R)-2-N-(7-Chloroquinolin-4-yl)cyclohexane-1,2-diamine ZINC38050616	93453548	0.946	
CQ2	(1S,2S)-2-N-(7-chloroquinolin-4-yl)cyclohexane-1,2-diamine ZINC38050615	57227818	0.95	
CQ3	N'-(7-chloroquinolin-4-yl)-N-cyclohexylethane-1,2-diamine	224506	0.957	

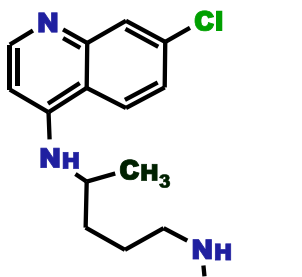
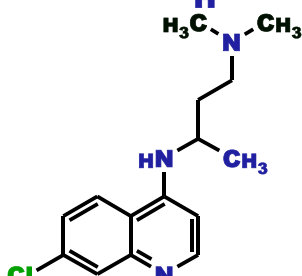
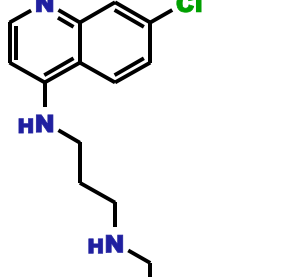
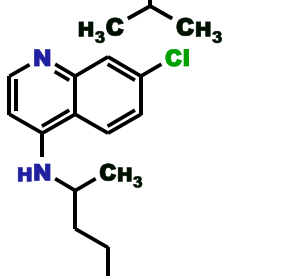
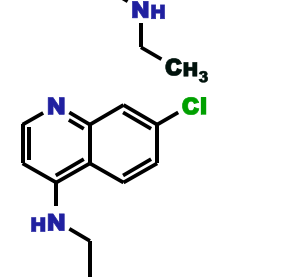
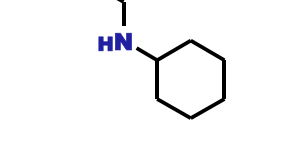
(continued on next page)

Table 1 (continued)

Compounds	IUPAC Name & ZINC Id	PubChem CID	Tanimoto Coefficient	Chemical Structures
	ZINC01683221			
CQ4	N-(4-aminobutyl)-7-chloroquinolin-4-amine ZINC19721342	11770817	0.946	
CQ5	(1R,2S)-2-N-(7-chloroquinolin-4-yl)cyclohexane-1,2-diamine ZINC38050617	93453549	0.952	
CQ6	N'-(7-Chloroquinolin-4-yl)-N-ethylpropane-1,3-diamine ZINC01709131	273882	0.933	
CQ7	N-(7-Chloroquinolin-4-yl)-N',N'-dimethylbutane-1,4-diamine ZINC01729567	3728380	0.984	
CQ8	N4-(7-chloroquinolin-4-yl)-n1-methylpentane-1,4-diamine ZINC02042606	225111	0.989	

(continued on next page)

Table 1 (continued)

Compounds	IUPAC Name & ZINC Id	PubChem CID	Tanimoto Coefficient	Chemical Structures
CQ9	Didesethyl Chloroquine ZINC06020572	122672	0.974	
CQ10	3-N-(7-chloroquinolin-4-yl)-1-N,1-N-dimethylbutane-1,3-diamine ZINC06176159	4065492	0.959	
CQ11	N'-(7-Chloroquinolin-4-yl)-N-(2-methylpropyl)propane-1,3-diamine ZINC01706242	223166	0.946	
CQ12	Desethyl Chloroquine ZINC02042694	95478	0.993	
CQ13	N'-(7-chloroquinolin-4-yl)-N-cyclohexylpropane-1,3-diamine ZINC01596768	225119	0.975	
CQ14	1-(7-Chloroquinolin-4-yl)-N,N-dimethylpiperidin-3-amine ZINC78617773	60291042	0.974	

(continued on next page)

Table 1 (continued)

Compounds	IUPAC Name & ZINC Id	PubChem CID	Tanimoto Coefficient	Chemical Structures
CQ15	N-(7-chloroquinolin-4-yl)-N',N'-diethylpropane-1,3-diamine ZINC01542123	3805581	0.962	
CQ16	(3R)-1-(7-chloroquinolin-4-yl)azepan-3-amine ZINC82133910	96578389	0.947	
CQ17	N-(7-chloroquinolin-4-yl)-N'-propan-2-ylpropane-1,3-diamine ZINC01706241	223165	0.945	
CQ18	1-(7-chloroquinolin-4-yl)azepan-3-amine ZINC82133908	70760365	0.945	
CQ19	N-(7-Chloroquinolin-4-yl)-N',N'-di(propan-2-yl)ethane-1,2-diamine ZINC20552561	11962135	0.919	

(continued on next page)

Table 1 (continued)

Compounds	IUPAC Name & ZINC Id	PubChem CID	Tanimoto Coefficient	Chemical Structures
CQ20	N-(7-chloroquinolin-4-yl)-N',N'-dimethylpropane-1,3-diamine ZINC01542122	11608635	0.915	
CQ21	N'-(7-Chloroquinolin-4-yl)-N,N-diethylethane-1,2-diamine ZINC0006792	408190	0.907	
CQ22	1-N-(7-Chloroquinolin-4-yl)-2-N,N-dimethylpropane-1,2-diamine ZINC37985881	11507234	0.906	
CQ23	(1-Quinolin-4-ylpiperidin-4-yl) methanamine ZINC44514898	61785796	0.904	
CQ24	N-(6-Chloroquinolin-4-yl)-N',N'-diethylpropane-1,3-diamine ZINC01596764	408567	0.899	

(continued on next page)

Table 1 (continued)

Compounds	IUPAC Name & ZINC Id	PubChem CID	Tanimoto Coefficient	Chemical Structures
CQ25	N-(7-Chloroquinolin-4-yl)-N'-methylpropane-1,3-diamine ZINC06746756	6472985	0.88	
CQ26	(E)-N-(7-Chloroquinolin-4-yl)-N',N'-diethylbut-2-ene-1,4-diamine ZINC33956413	10093137	0.878	
CQ27	7-Chloro-N-(5-pyrrolidin-1-ylpentan-2-yl)quinolin-4-amine ZINC08579986	220624	0.869	

analogues were performed using density functional theory (DFT) B3LYP with 6-31 + G (d, p) basis set using Gaussian 16 suite [46]. In the current study, global reactivity descriptors such as ionization potential, electron affinity, chemical potential (μ), electronegativity (χ), chemical hardness (η), and electrophilicity (ω) were calculated [47,48]. The basicity and acidity parameters [49,50] were predicted as mentioned in equations (1) and (2) to understand the reactivity of the selected compounds as compared to those of CQ and HCQ.

$$\text{Basicity} = \eta/2\chi \quad (\text{Eq. 1})$$

$$\text{Acidity} = \chi/2\eta \quad (\text{Eq. 2})$$

Where η = chemical hardness; χ = electronegativity.

3. Results and discussion

We collected a total of 800 analogues of CQ and HCQ from the ZINC database of the webserver SwissSimilarity and performed similarity

ranking analysis. Based on the Tanimoto coefficient analysis, 32 analogues (28 CQ and 4 HCQ) were selected with a similarity score above 0.85 for further screening. Details of these analogues of CQ and HCQ with their similarity score, ZINC ID, IUPAC name, and chemical structures are listed in Table 1 and respective SMILES are given in the supplementary data of Table 1.

Drug-likeness involves various structural features and molecular properties that determine how similar a particular ligand molecule is to the known drugs. These filters are important in drug discovery to design derivatives/analogues within the purview of drug-likeness space [51]. From the similar compounds identified, the 4 analogues of HCQ and 25 out of 28 analogues of CQ do not violate any of the drug-likeness rules. Three analogues of CQ (ZINC01596768, ZINC01706242, and ZINC20552561) violated the Muegge rule, so these three were omitted for further analysis. The bioavailability of ligands was predicted using the swissADME tool [28]. Bioavailability is the concentration of a drug that can be absorbed by the body with respect to the systemic circulation and total dose. The bioavailability prediction score of a compound

Table 2

Prediction of ADMET profile for HCQ and CQ analogues. The green colour indicates Blood-Brain Barrier (BBB) and Human Intestinal Absorption (HIA): Positive, P-glycoprotein Inhibitor (PGI): Non-inhibitor, CYP Inhibitory Promiscuity (CYP): Low, Carcinogens (C): Non-carcinogens and Aqueous solubility (AS): 0 to -4). The red colour indicates inhibitors of P-glycoprotein and Cytochrome P450 and high aqueous solubility.

Compounds	Blood-Brain Barrier	Human Intestinal Absorption	P-glycoprotein Inhibitor	CYP Inhibitory Promiscuity	Carcinogens	Aqueous Solubility
HCQ1	Positive	Positive	Non-inhibitor	Low	Non-carcinogens	-3.70
HCQ2	Positive	Positive	Inhibitor	High	Non-carcinogens	-3.84
HCQ3	Positive	Positive	Inhibitor	High	Non-carcinogens	-3.59
HCQ4	Positive	Positive	Inhibitor	Low	Non-carcinogens	-3.93
CQ1	Positive	Positive	Non-inhibitor	Low	Non-carcinogens	-3.33
CQ2	Positive	Positive	Non-inhibitor	Low	Non-carcinogens	-3.33
CQ3	Positive	Positive	Non-inhibitor	Low	Non-carcinogens	-3.33
CQ4	Positive	Positive	Non-inhibitor	Low	Non-carcinogens	-3.31
CQ5	Positive	Positive	Non-inhibitor	Low	Non-carcinogens	-3.33
CQ6	Positive	Positive	Non-inhibitor	Low	Non-carcinogens	-3.57
CQ7	Positive	Positive	Non-inhibitor	Low	Non-carcinogens	-3.56
CQ8	Positive	Positive	Non-inhibitor	Low	Non-carcinogens	-3.34
CQ9	Positive	Positive	Non-inhibitor	Low	Non-carcinogens	-3.49
CQ10	Positive	Positive	Non-inhibitor	Low	Non-carcinogens	-3.95
CQ11	Positive	Positive	Non-inhibitor	High	Non-carcinogens	-3.46
CQ12	Positive	Positive	Non-inhibitor	Low	Non-carcinogens	-3.70
CQ13	Positive	Positive	Non-inhibitor	High	Non-carcinogens	-3.61
CQ14	Positive	Positive	Non-inhibitor	High	Non-carcinogens	-3.24
CQ15	Positive	Positive	Inhibitor	High	Non-carcinogens	-3.91
CQ16	Positive	Positive	Non-inhibitor	High	Non-carcinogens	-3.71
CQ17	Positive	Positive	Non-inhibitor	High	Non-carcinogens	-3.65
CQ18	Positive	Positive	Non-inhibitor	High	Non-carcinogens	-3.71
CQ19	Positive	Positive	Non-inhibitor	High	Non-carcinogens	-3.83
CQ20	Positive	Positive	Non-inhibitor	Low	Non-carcinogens	-3.67
CQ21	Positive	Positive	Non-inhibitor	High	Non-carcinogens	-3.56
CQ22	Positive	Positive	Non-inhibitor	High	Non-carcinogens	-3.58
CQ23	Positive	Positive	Non-inhibitor	High	Non-carcinogens	-2.98
CQ24	Positive	Positive	Inhibitor	High	Non-carcinogens	-3.91
CQ25	Positive	Positive	Non-inhibitor	High	Non-carcinogens	-3.32
CQ26	Positive	Positive	Non-inhibitor	High	Non-carcinogens	-4.21
CQ27	Positive	Positive	Inhibitor	High	Non-carcinogens	-4.02

ranges from 0 to 1. Low bioavailability of a compound is indicated by the value of less than 0.5, whereas if the value is above 0.5, the compound is predicted to have high bioavailability. Based on the results of the predicted bioavailability, all analogues showed higher bioavailability (bioavailability score: 0.55). Therefore, all these 31 candidate analogues were selected for further study.

Predicted ADMET properties of these 31 analogues are shown in

Table 2. Positive HIA of the selected analogues indicate that these molecules are highly absorbed in the human intestine. The BBB is also positive, signifying that these compounds could enter the blood-brain barrier. CYPs play a vital role in the metabolism of drugs by catalyzing their biotransformation which is responsible for their degradation and excretion [52]; it is necessary to identify CYP-inhibiting properties during development of a new drug. Most of the analogues resulting from

Table 3

Binding energy and the different types of interaction between the spike protein (PDB ID: 6LZG) of SAR-CoV-2 with CQ & HCQ and their analogues selected in the study.

Compounds	Binding Energy (kcal/mol)	Pi-Donor Hydrogen Bond	Pi-sigma	Pi-Alkyl Interaction	Pi-Pi T shaped	Pi-Pi Stacked	Pi-Anion	Van der Waals
HCQ	-3.98			Pro426, Phe464, Pro463, Glu516				
HCQ1	-6.83	Ser514		Pro426, Pro463, Tyr396	Phe464			
CQ	-4.38			Pro426, Asp428, Phe429, Pro463, Phe464				
CQ1	-7.29		Thr430	Pro426, Asp428, Pro463, Tyr396	Phe46, Phe515			Glu516
CQ2	-6.67			Pro426, Asp428, Tyr396		Phe464	Glu516	
CQ4	-6.07	Ser514		Pro426, Asp428, Phe464, Tyr396				
CQ3	-6.05		Trp436	Phe338, Phe342, Phe374, Leu368, Val367	Phe464			
CQ5	-6.03		Pro426	Asp428, Pro463	Phe464			
CQ9	-5.89			Tyr396, Pro426, Asp428, Pro463			Glu516	
CQ8	-5.26			Pro426, Asp428, Phe464,			Glu516	
CQ6	-5.15	Phe338		Lue335, Cys336, Val362, Asp364				
CQ12	-4.95			Asn343, Phe342, Leu368, Leu441		Phe374		
CQ10	-4.84			Tyr396, Pro426, Pro463	Phe464			
CQ20	-4.76		Ala372	Tyr369, Phe374				
CQ7	-4.49		Trp436	Val367, Leu368, Phe374				

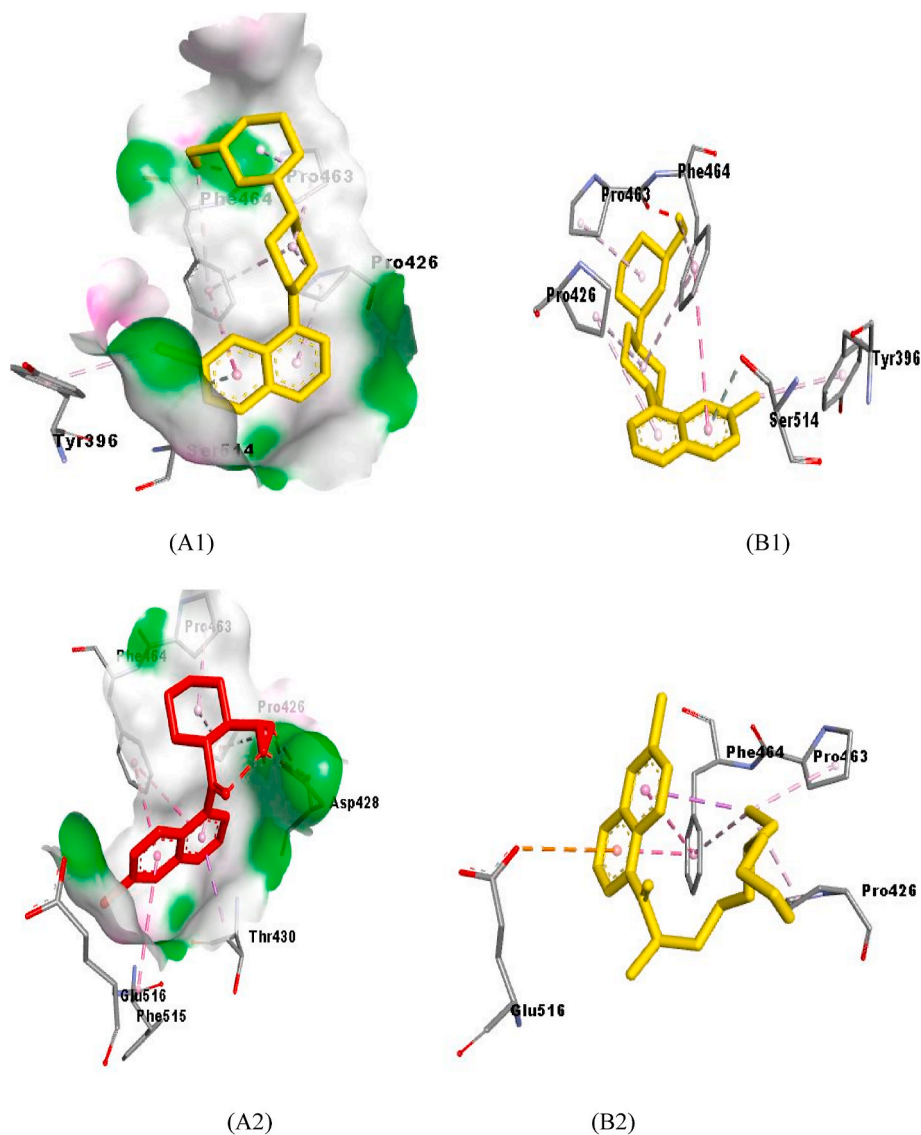


Fig. 1. View of the top-ranking analogues (A1-B1) HCQ1 and (A2-B2) CQ1 docked in the ligand-binding site of the SAR-CoV-2 spike protein receptor. (A) Ligands with spike protein (hydrophobicity surface) at the active binding site. (B) 3D view of ligands with surrounding amino acids of the spike protein of SAR-CoV-2.

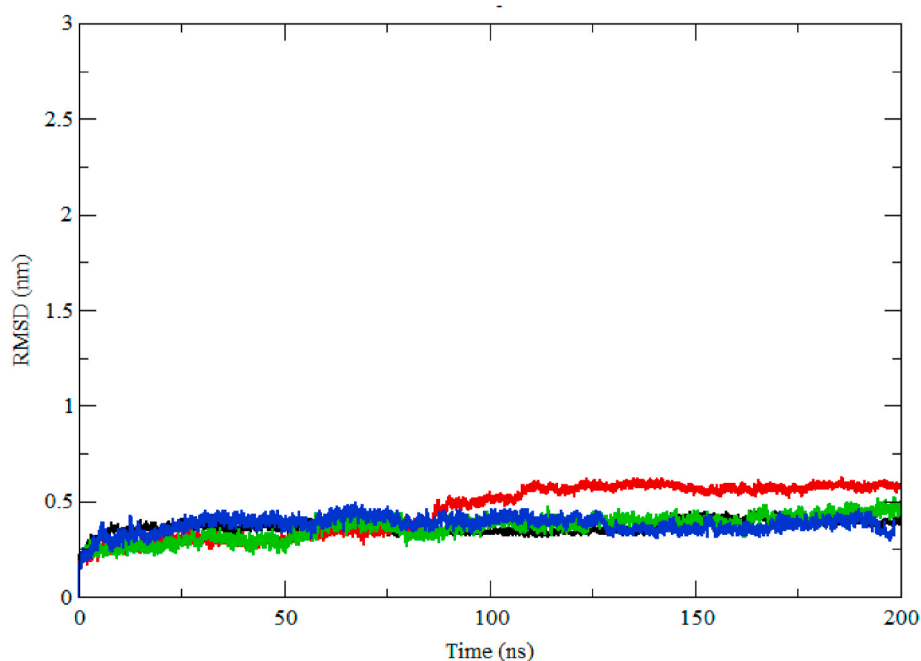


Fig. 2. The root mean square deviation (RMSD) graph for the parent and analogue drug – spike protein complexes. Colour scheme: CQ, black; HCQ, red; CQ1, green; HCQ1, blue.

drug-likeness have low CYP450 inhibitory properties, except HCQ2, HCQ3, and CQ14 to CQ18 and CQ20 to CQ27. All the analogues except HCQ2, HCQ3, HCQ4, CQ15, CQ24 and CQ27 are non-inhibitors of P-glycoprotein, so these 6 analogues were not considered for further analysis in the study. When the genotoxic criteria of all the drugs were evaluated, they were found to be non-carcinogenic. Therefore, it was determined that only 13 analogues (1 HCQ and 12 CQ) were suitable candidates for the development of potential alternative compounds for HCQ and CQ against COVID-19 viral targets.

The molecular docking studies showed that the spike glycoprotein interacts with HCQ1 through five amino acid residues, namely Pro426,

Pro463, Phe464, Ser514, and Tyr396 with a binding energy of -6.83 kcal/mol (Table 3, Fig. 1). In our study we found that the binding trend of the HCQ1 was higher than that of the parent drug; HCQ thus, this analogue displayed better binding affinity than that of the control drug. This analogue was found to interact with the binding pocket (Pro426, Pro463, Phe464, Ser514, Tyr396) as compared to that of the parent drug (Pro426, Phe464, Pro463, Glu516) suggesting similar interaction pattern. A pi-alkyl interaction occurs between HCQ1 and amino acid residues Pro426, Pro463 and Tyr396 of spike proteins. Conformational stability of the analogue HCQ1 is also associated with Pi-Pi T-shaped interactions with the amino acid residue, Phe464 and Pi-Donor

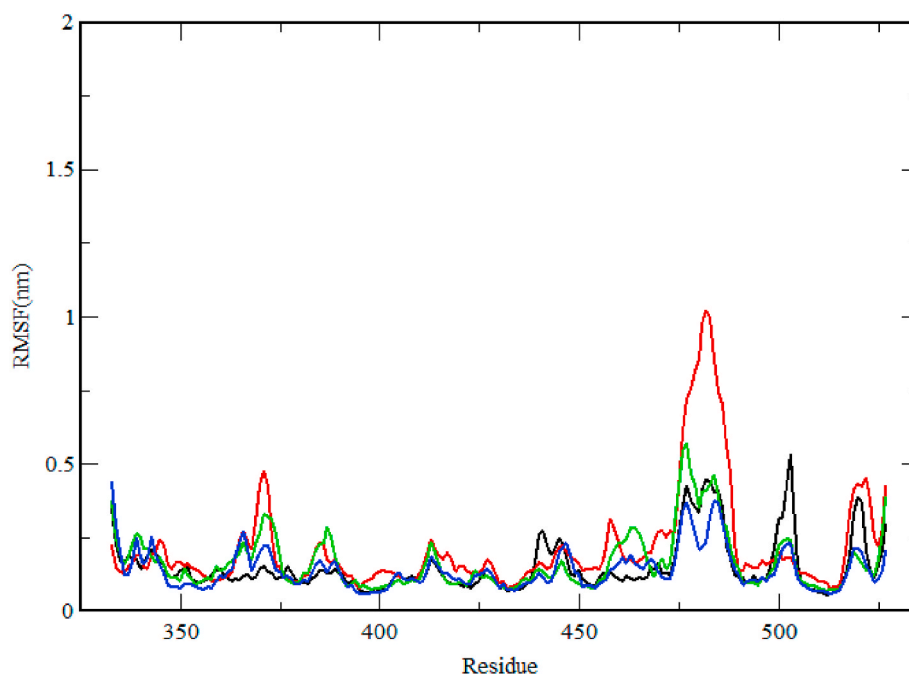


Fig. 3. The root mean square fluctuation (RMSF) graph for the drug-spike protein complexes. Colour scheme: CQ, black; HCQ, red; CQ1, green; HCQ1, blue.

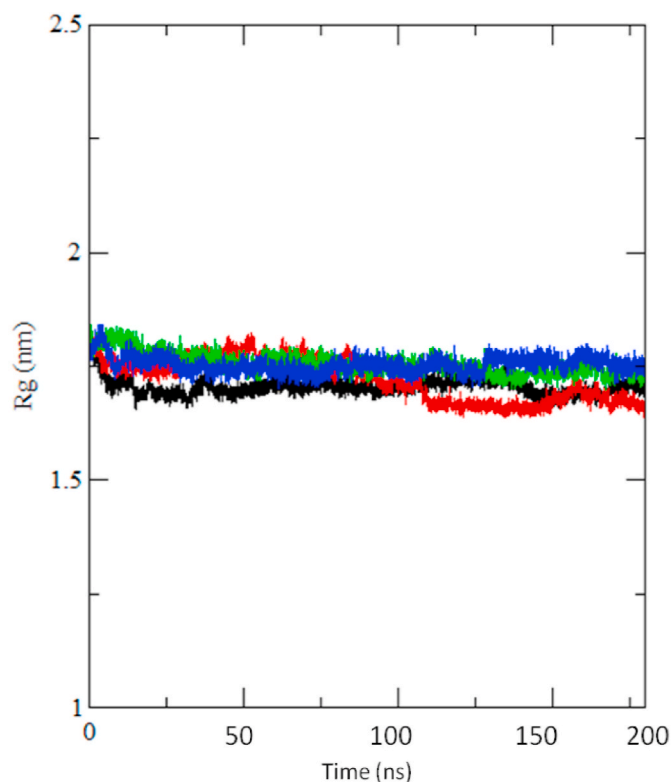


Fig. 4. The radius of gyration (Rg) plot for the drug-spike protein complexes. Colour scheme: CQ, black; HCQ1, red; CQ1, green; HCQ1, blue.

Hydrogen Bond with amino acid residue, Ser514.

Similarly, all the 12 analogues of CQ show a better binding affinity than that of the parent drug, and their binding energies are in the range between -4.49 kcal/mol and -7.29 kcal/mol. Among the CQ analogues, CQ1 (-7.29 kcal/mol), CQ2 (-6.67 kcal/mol) and CQ4 (-6.07 kcal/mol) were the ranking inhibitors of SARS-CoV-2 spike glycoprotein. (Table 3, Supplementary Figure 1). From the results so obtained, it is clear that HCQ analogue such as “1-[1-(6-Chloroquinolin-4-yl) piperidin-4-yl] piperidin-3-ol” and CQ analogue- (1R,2R)-2-N-(7-Chloroquinolin-4-yl)cyclohexane-1,2-diamine shows higher binding affinity with the spike protein of the SAR-CoV-2. The interaction of these ligands with the receptor protein has been depicted in Fig. 1 and Table 3. CQ1 has the highest binding affinity and interacts with Pro426, Asp428, Pro463, Phe464, Phe515, Thr430, Glu516, Tyr396 amino acid residues of the spike glycoprotein as shown in Fig. 1. The stability of CQ1 at the interaction site of the spike protein is attributed to the presence of various Pi-interactions, such as Pi-alkyl interaction with amino acid residues, Pro426, Asp428, Pro463, Tyr396, Pi-Pi interaction with amino acid residues, Phe464, Phe515, and Pi-Sigma interaction with amino acid residue Thr430. MD analysis was carried out for the stable complexes of CQ and HCQ and their analogues for a period of 200 ns simulations run to understand the dynamic behaviour of the spike protein and to compare the difference between the parent and the analogue drugs. RMSD was plotted to understand the stability of the protein-drug complexes. The average RMSD values were observed to be 0.36 nm, 0.45 nm, 0.36 nm and 0.38 nm for Spike-CQ, Spike-HCQ, Spike-CQ1 and Spike-HCQ1, respectively. The RMSD plot (Fig. 2) suggests that the binding of the Spike-CQ, Spike-CQ1, Spike-HCQ remain stable throughout the entire MD simulation period. A sudden fluctuation is seen in Spike-HCQ1 complex at around 80 ns, but afterwards it is stable again till the end of the simulations. The CQ1-spike complex showed higher stability than that of the HCQ1 during the entire 200 ns simulation run.

To gain an insight into the structural flexibility, root mean square

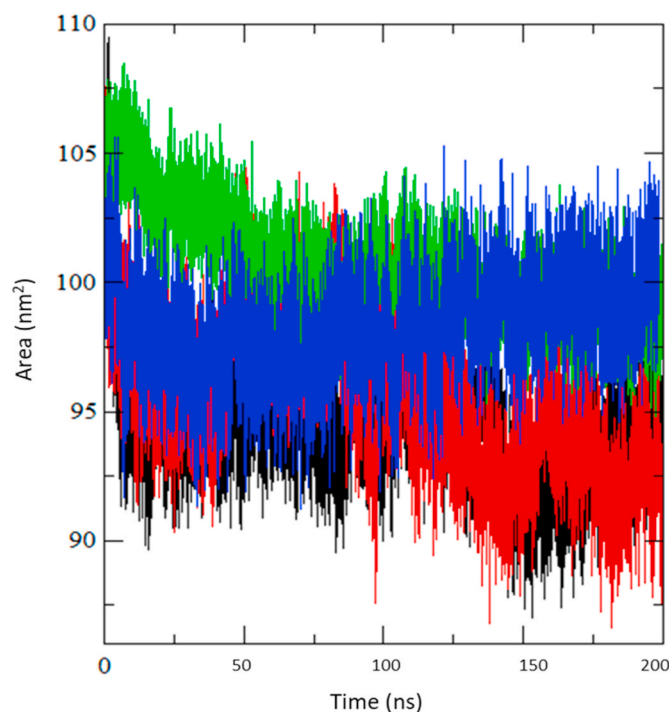


Fig. 5. The Solvent Accessible Surface Area (SASA) plot for the drug-spike protein complexes as a function of time. Colour scheme: CQ, black; HCQ1, red; CQ1, green; HCQ1, blue.

fluctuation (RMSF) was examined. RMSF of the backbone atoms of the residues was plotted against simulated trajectory (Fig. 3). The average RMSF for all the complexes was evaluated. The HCQ1-Spike complex was observed to be 0.14 nm and the fluctuation was observed to be higher, with an average of 0.18 nm in the CQ1-Spike complex. The plot indicates global changes rather than local changes. Both RMSD and RMSF emphasize the stability aspects of the spike protein which seems to be impacted by the interaction of these selected drugs.

The compactness of these complexes was also explored by analyzing their radius of gyration (Rg) values (Fig. 4). The average Rg values for CQ-Spike, HCQ-Spike, CQ1-Spike and HCQ1-Spike were observed to be 1.70 nm, 1.72 nm, 1.75 nm and 1.74 nm, respectively. The binding of the analogues showed higher Rg values than those of the parent drug. Lower Rg values were reported in case of CQ-Spike and HCQ-Spike complexes. A higher Rg value for selected analogues CQ1 and HCQ1 was obtained in comparison to the parent CQ & HCQ-spike protein complexes indicating that the spike protein structure is considerably affected leading to the inhibition of cascading events. The solvent-accessible surface area (SASA) is characterized by the region of a protein accessible to solvent molecules. The average SASA values for CQ-Spike, HCQ-Spike, CQ1-Spike and HCQ1-Spike were 94.57 nm², 95.51 nm², 100.68 nm², and 97.58 nm² respectively during the 200 ns MD simulations. Results showed a comparable range in SASA values as observed with different spike complexes, particularly in Spike-CQ1 and Spike-HCQ1 complexes, which showed higher SASA values, whereas parent drugs CQ and HCQ with spike show lower SASA value (see Fig. 5).

We also studied the collective motion of the analogues (HCQ1 and CQ1) and parent drugs (HCQ and CQ) with spike protein from their MD trajectories using principal component analysis (PCA). PCA was examined for understanding the structural and conformational changes in spike protein due to the binding of analogues and parent drugs. In this method, the dynamics of CQ-Spike, CQ1-Spike, HCQ-Spike and HCQ1-Spike were ascertained utilizing gmxc covar module with reference to the backbone. The atomic fluctuations during eigenvector calculation

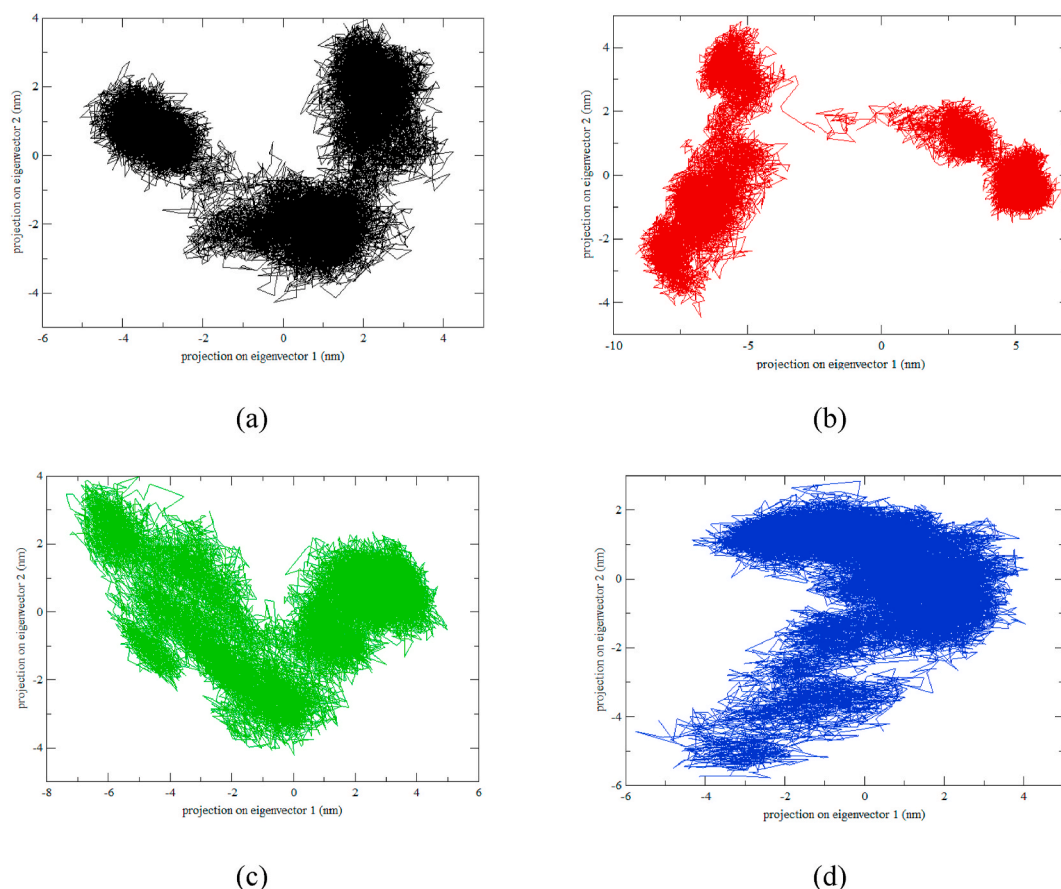


Fig. 6. 2D projection of trajectories on eigenvectors showed different projections of spike protein in case of (a) Spike-CQ (b) Spike-HCQ (c) Spike-CQ1 and (d) Spike-HCQ1. Colour scheme: CQ, black; HCQ, red; CQ1, green; HCQ1, blue.

were also reported in this study. The 2D projection of eigenvectors indicated diverse projections of spike protein upon binding with different molecules of ligands (Fig. 6). This analysis indicated the random fluctuations in the atoms of spike protein upon binding of different ligands and also suggests that the distinct positions in the spike protein undergo conformational changes.

To visualize the energy minima landscape of CQ, CQ1, HCQ and HCQ1 bound spike protein, we studied the free energy landscape (FEL) against first two principal components, Rg and RMSD which revealed ΔG value from 0 to 10 kJ/mol (Fig. 7). The shape and size of the minimal energy area (shown in blue) indicate the stability of the protein and protein-ligand complexes. Compact, unscattered and more centralized blue areas indicate the stability of the protein complex. Fig. 7 suggests that the analogue CQ1 bound spike complex is more stable than that of its parent drug, CQ-spike complex, and also than that HCQ and HCQ1 bound spike protein. Thus these analogues have the potential to induce spike protein to enter the local energy minimal state.

The basicity and acidity values for the listed top-ranking docked derivatives of HCQ and CQ including the parent compounds are falling in the range of 1.22–1.30 and 3.05 to 3.25, respectively (Table 4). This reflects that the analogues also exhibit similar biochemical response on viral inhibition by endosomal acidification to stop viral replication [45]. Thus, our study suggests that these selected analogues have a higher potential to work effectively as a novel antiviral analogue drug as compared to that of CQ and HCQ.

4. Conclusions

Developing a robust framework for finding a desirable compound that binds and inhibits the attachment/internalization of SARS-CoV-2

might lead to potential therapeutics. This will overcome time constraints on antiviral drug discovery processes. Computational predictive approaches have been effectively used to develop a faster prospective drugs or inhibitor candidates. In this study, we demonstrated an integrated computational screening framework to identify drug molecules that selectively target the spike protein of SARS-CoV-2 as a potent and safer alternative for CQ and HCQ. Virtual screening of similar compound libraries of CQ and HCQ was performed and the screened compounds along with parent drugs have been evaluated for drug likeness, ADMET properties, molecular docking and molecular dynamics simulations. Our docking study revealed that the identified analogue CQ1 has better binding affinity than that of HCQ1 and also that of parent drugs. Subsequently, MD simulations and PCA analysis of these complexes reform the stability of its mode of binding and thereby, inhibiting the activity of spike protein. Our findings suggest that the systematic selection of SARS-CoV-2 inhibitors was carried out by narrowing down on compounds and identifying from among them a suitable drug for COVID-19 treatment.

Author's contribution

RP, MS, and AG designed the study. PS, SSC, SP, MS, SG, and AG carried out the *in silico* work. MS, AG and SG wrote the manuscript, carried out data analysis for tabulation and prepared the figures. All the authors read and approved the final manuscript.

Declaration of competing interest

The authors declare that they have no known competing financial interests or personal relationships that could have appeared to influence the work reported in this paper.

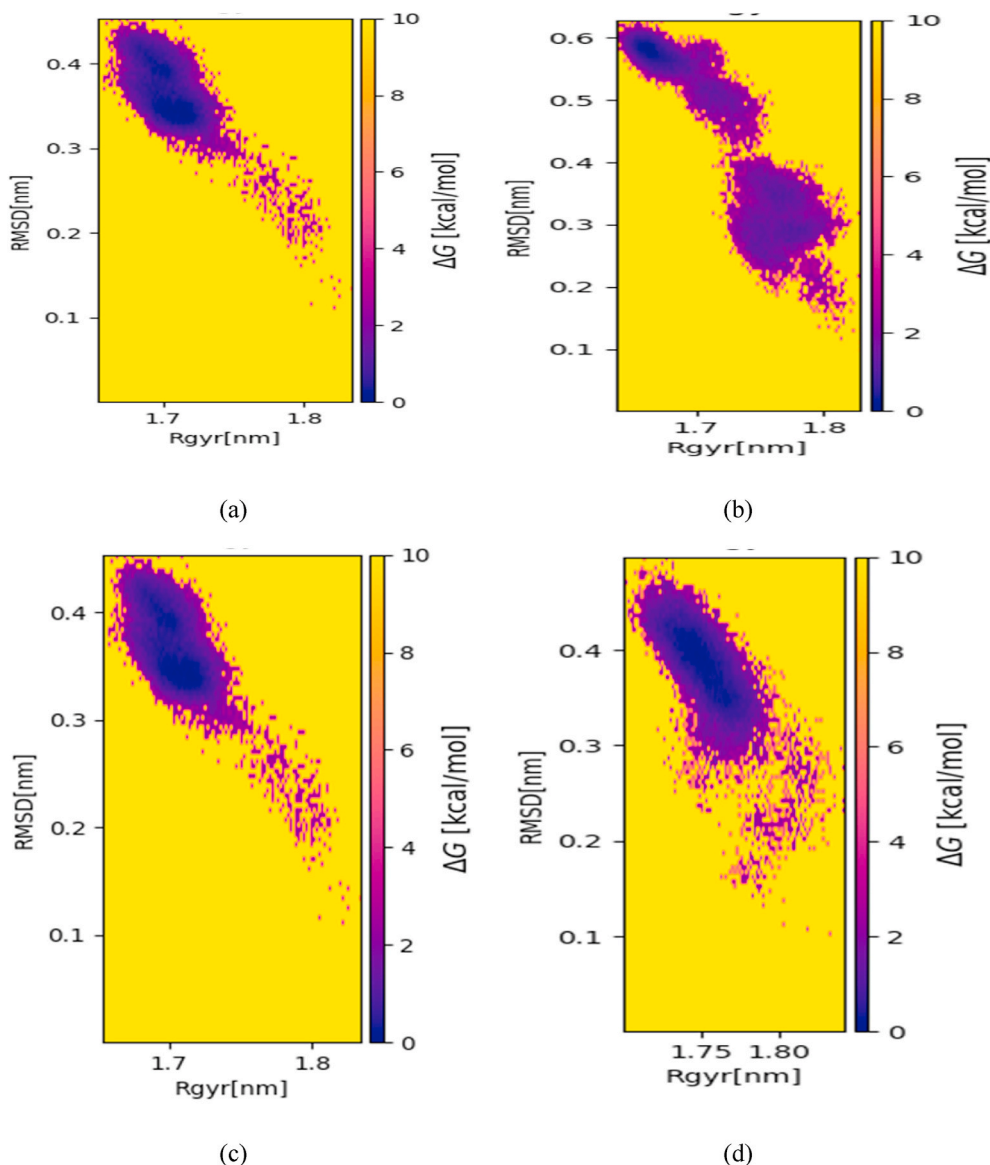


Fig. 7. Free Energy Landscape (FEL in kcal/mol) of the first two principal components for (a) Spike-CQ (b) Spike-HCQ (c) Spike-CQ1 and (d) Spike-HCQ1.

Table 4

Calculated acidity and basicity of CQ & HCQ and their analogues.

Compounds	Basicity	Acidity
HCQ	1.26	3.25
HCQ1	1.23	3.20
CQ	1.27	3.16
CQ1	1.24	3.31
CQ2	1.24	3.24
CQ4	1.26	3.23
CQ3	1.23	3.24
CQ5	1.30	3.04

Acknowledgements

The authors thank the CSIR-Indian Institute of Toxicology Research, Lucknow and Council of Scientific and Industrial Research, New Delhi for the support under MLP-003 project (Food, Drug and Chemical Toxicology) and CSIR Development of Repurposed Drugs/New Drugs & Vaccine vertical for COVID-19 mitigation. MS is thankful to the Department of Science and Technology, New Delhi for providing INSPIRE fellowship. CSIR-IITR manuscript communication no. 3675.

Appendix B. Supplementary data

Supplementary data to this article can be found online at <https://doi.org/10.1016/j.compbmed.2021.104222>.

References

- [1] J.S. Mackenzie, D.W. Smith, COVID-19: a novel zoonotic disease caused by a coronavirus from China: what we know and what we don't, *Microbiology Australia* 41 (2020) 45–50.
- [2] C.A. Devaux, J.-M. Rolain, P. Colson, D. Raoult, New insights on the antiviral effects of chloroquine against coronavirus: what to expect for COVID-19? *Int. J. Antimicrob. Agents* (2020) 105938.
- [3] F. Touret, X. de Lamballerie, Of Chloroquine and COVID-19, *Antiviral research*, 2020, p. 104762.
- [4] M. Wang, R. Cao, L. Zhang, X. Yang, J. Liu, M. Xu, Z. Shi, Z. Hu, W. Zhong, G. Xiao, Remdesivir and chloroquine effectively inhibit the recently emerged novel coronavirus (2019-nCoV) in vitro, *Cell Res.* 30 (2020) 269–271.
- [5] P. Colson, J.M. Rolain, J.C. Lagier, P. Brouqui, D. Raoult, Chloroquine and hydroxychloroquine as available weapons to fight COVID-19, *Int. J. Antimicrob. Agents* 55 (2020) 105932.
- [6] F. Diaz-Griffero, S.A. Hoschander, J. Brojatsch, Endocytosis is a critical step in entry of subgroup B avian leukosis viruses, *J. Virol.* 76 (2002) 12866–12876.
- [7] D. Ferreira, M. Santo, M. Rebello, M. Rebello, Weak bases affect late stages of Mayaro virus replication cycle in vertebrate cells, *J. Med. Microbiol.* 49 (2000) 313–318.

- [8] D. Gonzalez-Dunia, B. Cubitt, J.C. de la Torre, Mechanism of Borna disease virus entry into cells, *J. Virol.* 72 (1998) 783–788.
- [9] J. Liu, R. Cao, M. Xu, X. Wang, H. Zhang, H. Hu, Y. Li, Z. Hu, W. Zhong, M. Wang, Hydroxychloroquine, a less toxic derivative of chloroquine, is effective in inhibiting SARS-CoV-2 infection in vitro, *Cell discovery* 6 (2020) 1–4.
- [10] N. Mustafa, Therapeutic Preferences for Coronavirus 2 (SARS-CoV-2) Patients, 2020.
- [11] C. Ros, C.J. Burkhardt, C. Kempf, Cytoplasmic trafficking of minute virus of mice: low-pH requirement, routing to late endosomes, and proteasome interaction, *J. Virol.* 76 (2002) 12634–12645.
- [12] J.J. Kwiek, T.A. Haystead, J. Rudolph, Kinetic mechanism of quinone oxidoreductase 2 and its inhibition by the antimalarial quinolines, *Biochemistry* 43 (2004) 4538–4547.
- [13] M.J. Vincent, E. Bergeron, S. Benjannet, B.R. Erickson, P.E. Rollin, T.G. Ksiazek, N. G. Seidah, S.T. Nichol, Chloroquine is a potent inhibitor of SARS coronavirus infection and spread, *Virol. J.* 2 (2005) 1–10.
- [14] E. Schrezenmeier, T. Dörner, Mechanisms of action of hydroxychloroquine and chloroquine: implications for rheumatology, *Nat. Rev. Rheumatol.* (2020) 1–12.
- [15] M.A. Tortorici, A.C. Walls, Y. Lang, C. Wang, Z. Li, D. Koerhuis, G.-J. Boons, B.-J. Bosch, F.A. Rey, R.J. de Groot, Structural basis for human coronavirus attachment to sialic acid receptors, *Nat. Struct. Mol. Biol.* 26 (2019) 481–489.
- [16] M. Khan, S. Santhosh, M. Tiwari, P. Lakshmana Rao, M. Parida, Assessment of in vitro prophylactic and therapeutic efficacy of chloroquine against Chikungunya virus in vero cells, *J. Med. Virol.* 82 (2010) 817–824.
- [17] V.B. Randolph, G. Winkler, V. Stollar, Acidotropic amines inhibit proteolytic processing of flavivirus prM protein, *Virology* 174 (1990) 450–458.
- [18] A.M. Hashem, B.S. Alghamdi, A.A. Algaissi, F.S. Alshehri, A. Bukhari, M.A. Alfaleh, Z.A. Memish, Therapeutic Use of Chloroquine and Hydroxychloroquine in COVID-19 and Other Viral Infections: A Narrative Review, *Travel Medicine and Infectious Disease*, 2020, p. 101735.
- [19] L. Mittal, L. Zhang, R. Feng, V.P. Werth, Antimalarial drug toxicities in patients with cutaneous lupus and dermatomyositis: a retrospective cohort study, *J. Am. Acad. Dermatol.* 78 (2018) 100–106, e101.
- [20] R. Choudhary, A.K. Sharma, Potential Use of Hydroxychloroquine, Ivermectin and Azithromycin Drugs in Fighting COVID-19: Trends, Scope and Relevance, *New Microbes and New Infections*, 2020, p. 100684.
- [21] E.W. McChesney, Animal toxicity and pharmacokinetics of hydroxychloroquine sulfate, *Am. J. Med.* 75 (1983) 11–18.
- [22] M.T. Pelle, J.P. Callen, Adverse cutaneous reactions to hydroxychloroquine are more common in patients with dermatomyositis than in patients with cutaneous lupus erythematosus, *Arch. Dermatol.* 138 (2002) 1231–1233.
- [23] R. Tailor, I. Elaraoud, P. Good, M. Hope-Ross, R. Scott, A case of severe hydroxychloroquine-induced retinal toxicity in a patient with recent onset of renal impairment: a review of the literature on the use of hydroxychloroquine in renal impairment, *Case Rep Ophthalmol Med* 2012 (2012) 182747.
- [24] J.J. Irwin, B.K. Shoichet, ZINC— a free database of commercially available compounds for virtual screening, *Journal of chemical information and modelling* 45 (2005) 177–182.
- [25] V. Zoete, A. Daina, C. Bovigny, O. Michielin, SwissSimilarity: a Web Tool for Low to Ultra High Throughput Ligand-Based Virtual Screening, ACS Publications, 2016.
- [26] P. Willett, Similarity-based virtual screening using 2D fingerprints, *Drug Discov. Today* 11 (2006) 1046–1053.
- [27] S. Kim, P.A. Thiessen, E.E. Bolton, J. Chen, G. Fu, A. Gindulyte, L. Han, J. He, S. He, B.A. Shoemaker, PubChem substance and compound databases, *Nucleic Acids Res.* 44 (2016) D1202–D1213.
- [28] A. Daina, O. Michielin, V. Zoete, SwissADME: a free web tool to evaluate pharmacokinetics, drug-likeness and medicinal chemistry friendliness of small molecules, *Sci. Rep.* 7 (2017) 42717.
- [29] D.R. Loureiro, J.X. Soares, J.C. Costa, Á.F. Magalhães, C.M. Azevedo, M.M. Pinto, C.M. Afonso, Structures, activities and drug-likeness of anti-infective xanthone derivatives isolated from the marine environment: a review, *Molecules* 24 (2019) 243.
- [30] F. Cheng, W. Li, Y. Zhou, J. Shen, Z. Wu, G. Liu, P.W. Lee, Y. Tang, admetSAR: a Comprehensive Source and Free Tool for Assessment of Chemical ADMET Properties, ACS Publications, 2012.
- [31] F. Li, Structure, function, and evolution of coronavirus spike proteins, *Annual review of virology* 3 (2016) 237–261.
- [32] Q. Wang, Y. Zhang, L. Wu, S. Niu, C. Song, Z. Zhang, G. Lu, C. Qiao, Y. Hu, K.-Y. Yuen, Structural and Functional Basis of SARS-CoV-2 Entry by Using Human ACE2, *Cell*, 2020.
- [33] H. Berman, K. Henrick, H. Nakamura, J.L. Markley, The worldwide Protein Data Bank (wwPDB): ensuring a single, uniform archive of PDB data, *Nucleic Acids Res.* 35 (2007) D301–D303.
- [34] D.S. Biovia, Discovery Studio Modeling Environment, Release, San Diego, 2017. DassaultSystèmes, 2016, Available from:(Accessed 1 September 2016), (2016).
- [35] A.P. Norgan, P.K. Coffman, J.-P.A. Kocher, D.J. Katzmann, C.P. Sosa, Multilevel parallelization of AutoDock 4.2, *J. Cheminf.* 3 (2011) 12.
- [36] J. Racine, The Cygwin tools: a GNU toolkit for Windows, *J. Appl. Econom.* 15 (2000) 331–341.
- [37] H.J. Berendsen, D. van der Spoel, R. van Drunen, GROMACS: a message-passing parallel molecular dynamics implementation, *Comput. Phys. Commun.* 91 (1995) 43–56.
- [38] A.W. Schüttelkopf, D.M. Van Aalten, PRODRG: a tool for high-throughput crystallography of protein-ligand complexes, *Acta Crystallogr. Sect. D Biol. Crystallogr.* 60 (2004) 1355–1363.
- [39] N. Baildya, N.N. Ghosh, A.P. Chattopadhyay, Inhibitory activity of hydroxychloroquine on COVID-19 main protease: an insight from MD-simulation studies, *J. Mol. Struct.* (2020) 128595.
- [40] S.S. Ahmad, M. Sinha, K. Ahmad, M. Khalid, I. Choi, Study of caspase 8 inhibition for the management of alzheimer's disease: a molecular docking and dynamics simulation, *Molecules* 25 (2020) 2071.
- [41] B. Hess, H. Bekker, H.J. Berendsen, J.G. Fraaije, LINC: a linear constraint solver for molecular simulations, *J. Comput. Chem.* 18 (1997) 1463–1472.
- [42] J. Lemkul, From proteins to perturbed Hamiltonians: a suite of tutorials for the GROMACS-2018 molecular simulation package [article v1. 0], *Living Journal of Computational Molecular Science* 1 (2018) 5068.
- [43] E. Papaleo, P. Meregghetti, P. Fantucci, R. Grandori, L. De Gioia, Free-energy landscape, principal component analysis, and structural clustering to identify representative conformations from molecular dynamics simulations: the myoglobin case, *J. Mol. Graph. Model.* 27 (2009) 889–899.
- [44] S. Gupta, A.K. Singh, P.P. Kushwaha, K.S. Prajapati, M. Shuaib, S. Senapati, S. Kumar, Identification of potential natural inhibitors of SARS-CoV2 main protease by molecular docking and simulation studies, *J. Biomol. Struct. Dyn.* (2020) 1–19.
- [45] M.A.A. Al-Bari, Targeting endosomal acidification by chloroquine analogs as a promising strategy for the treatment of emerging viral diseases, *Pharmacol Res Perspect* 5 (2017) e00293. -e00293.
- [46] M. Frisch, G. Trucks, H. Schlegel, G. Scuseria, M. Robb, J. Cheeseman, G. Scalmani, V. Barone, G. Petersson, H. Nakatsuji, Gaussian 16, Gaussian, Inc., Wallingford, CT, 2016.
- [47] R. Parthasarathi, V. Subramanian, D.R. Roy, P. Chattaraj, Electrophilicity index as a possible descriptor of biological activity, *Bioorg. Med. Chem.* 12 (2004) 5533–5543.
- [48] R.G. Pearson, J. Songstad, Application of the principle of hard and soft acids and bases to organic chemistry, *J. Am. Chem. Soc.* 89 (1967) 1827–1836.
- [49] A.M. Socha, R. Parthasarathi, J. Shi, S. Pattathil, D. Whyte, M. Bergeron, A. George, K. Tran, V. Stavila, S. Venkatachalam, Efficient biomass pretreatment using ionic liquids derived from lignin and hemicellulose, in: *Proceedings of the National Academy of Sciences* vol. 111, 2014, pp. E3587–E3595.
- [50] A.A. Oliferenko, P.V. Oliferenko, J.G. Huddleston, R.D. Rogers, V.A. Palyulin, N. S. Zefirov, A.R. Katritzky, Theoretical scales of hydrogen bond acidity and basicity for application in QSAR/QSPR studies and drug design. Partitioning of aliphatic compounds, *J. Chem. Inf. Comput. Sci.* 44 (2004) 1042–1055.
- [51] N.A. Meanwell, Improving drug design: an update on recent applications of efficiency metrics, strategies for replacing problematic elements, and compounds in nontraditional drug space, *Chem. Res. Toxicol.* 29 (2016) 564–616.
- [52] A.H. Natalia, U.S.F. Tambunan, Screening of terpenoids as potential therapeutics against Zaire ebolavirus infection through pharmacophore-based drug design, *F1000Research* 8 (2019) 1040.